

Static and Dynamic Testing of Large-Amplitude Rotary Induced-Strain (LARIS Mk 2) Actuator

VICTOR GIURGIUTIU* AND CRAIG A. ROGERS

University of South Carolina, Mechanical Engineering Department, Columbia, SC 29208

SHANE MCNEIL

California State Polytechnic University, Mechanical Engineering Department, Pomona, CA 91768

ABSTRACT: A new concept for obtaining large-amplitude rotary displacements from small linear displacements generated by induced-strain active material stacks is considered. The concept utilizes the theory of twist-warping coupling in thin-wall open tubes. A large-displacement induced-strain rotary actuator, LARIS Mk 2, was built and tested under static and dynamic conditions. A rotary displacement of 6° was measured over a 0–50 Hz frequency range. The frequency response was found to be flat up to 40 Hz, and then increasing in the 40–50 Hz frequency range.

The theoretical development of the torsional vibration response for the LARIS Mk 2 actuator is also given. The derivation is performed in a general format for a body with distributed elastic and inertia parameters, and with generic boundary conditions consisting of root stiffness and tip angular deflection. The results of this theoretical analysis are confirmed by experimental measurements. The theory presented is versatile and can be used for the analysis of other torsional vibration devices with specific root and tip boundary conditions.

This LARIS concept presented in this paper can be successfully used in a series of aerospace and mechanical engineering applications, as for example in the actuation of adaptive control surfaces for aircraft wings and helicopter blades, or as rotary vane actuators in the control of turbomachinery exhaust flow for active reduction of turbulence, vibrations, and noise.

INTRODUCTION

SOLID-STATE induced-strain actuators present outstanding advantages over conventional electro-mechanical and hydraulic actuation due to their compact construction, very low parts count and potentially high reliability. Induced-strain materials can produce very large forces and, hence, large energy density, but small actual displacements (Giurgiutiu, Chaudhry, and Rogers, 1996). For most practical applications, amplification of the induced-strain displacement is needed. For rotary actuation, an additional mechanism must be provided to convert the linear induced-strain displacement into angular stroke output (Giurgiutiu, Chaudhry, Rogers; 1994; Straub and King, 1996). To minimize displacement losses, solid-state devices for amplification and angular-to-rotary conversion are preferred. Several attempts to produce twist of closed-tube structures using induced-strain actuators have been reported (Chen and Chopra, 1993; Bothwell, Chandra, and Chopra, 1994; Bernhard and Chopra, 1996) but with tip rotations that did not exceed 0.5° . These values are about an order of magnitude less than the values required to achieve meaningful practical results. The inability of these initial attempts at solid-state rotary actuation to achieve large angular displacement can be traced to a com-

mon cause: the use of closed-tube constructions that have inherently high torsional stiffness, and hence are difficult to deform.

A completely different approach is taken in the LARIS design concept (Giurgiutiu and Rogers, 1997). This concept utilizes an until-now unexplored application of basic solid-mechanics principles: the twist-warping coupling in open thin-wall tubes. The displacement amplification and the linear-to-rotary conversion are combined into one solid-state construction that can be easily manufactured. This paper reports new theoretical developments and experimental results obtained on an improved LARIS Mk 2 actuator that was recently designed, built, and subjected to extensive static and dynamic testing. The results showed 6° angular deflection over a 0–50 Hz frequency.

LARIS ACTUATOR OPERATING PRINCIPLE

The LARIS actuator converts small linear displacements into large angular displacements. The linear displacements are produced by an induced-strain actuator (Polytec PI P-245.70). The converter-amplifier is a thin-wall open tube that transforms the linear displacements to angular displacements. Figure 1 shows a detail of this thin-wall open tube. The thin-wall tube is called "open" since it has a longitudinal

*Author to whom correspondence should be addressed.

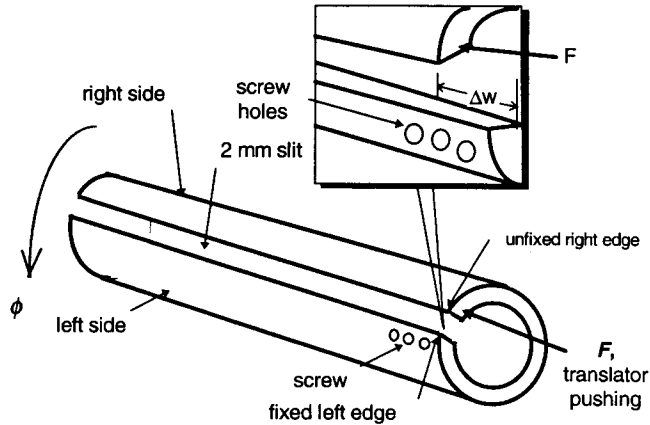


Figure 1. LARIS actuator open hollow tube that serves as displacement converter-amplifier for the LARIS actuator.

slit. The slit makes the tube exhibit the warping-torsion coupling effect (Giurgiutiu and Rogers, 1997).

The slit partitions the thin-wall tube into two: a left side and a right side. A two inch length portion of the tube left side is fastened to a housing unit with the aid of three screws. This fastening causes the left edge of the tube to become locally fixed. Under operation, the induced-strain actuator pushes on the unfixed right edge of the tube and causes a relative linear displacement, Δw , between the fixed and unfixed edges. The open-tube twist-warping coupling effect causes the relative linear displacement, Δw , to be converted into an angular rotation, ϕ . This angular rotation is readily apparent and increases in magnitude along the tube away from the root.

Using the theory of twist-warping coupling in thin-wall open tubes, Giurgiutiu and Rogers (1997) developed a linear kinematic relationship that describes the conversion-amplification of axial displacement into rotary displacement, i.e.,

$$\phi = \frac{L}{2A} \Delta w \quad (1)$$

where

ϕ = angular displacement (radian)

L = tube length (in or mm)

A = enclosed area, $\pi D^2/4$, where D is tube's mean diameter (mm² or in²)

Δw = relative displacement between tube's fixed and unfixed edges (in or mm)

Equation (1) states that, for a particular relative displacement, Δw , the angular displacement, ϕ , is proportional to the tube's length and inversely proportional to the tube's enclosed area.

For brevity, the static elasticity analysis deriving this equation will not be reproduced here and the reader is referred to Giurgiutiu and Rogers (1977). In the following sec-

tion we will concentrate our attention on the dynamic analysis and will develop the torsional vibration theory that describes the dynamic behavior of the LARIS actuator. The equations of motion will be stated. These equations will be used to derive a general vibration solution for arbitrary boundary conditions. The specific boundary conditions—root stiffness, tip inertia—will be imposed to yield the characteristic equation. The roots of the characteristic equation will be derived through a standard numerical method. For verification, two simple cases that have known closed form solutions (free-free and fixed-free) will be solved using the general characteristic equation and imposing asymptotic values for the root stiffness and tip inertia coefficients. Finally, comparison with experimental data will be used to confirm the theory.

TORSIONAL VIBRATION EQUATIONS

Figure 2 shows the schematic representation of the LARIS actuator used for torsional vibration analysis. The converter-amplifier open tube is represented by a uniform elastic bar of length L , torsional stiffness GJ , and distributed rotary inertia, I_p . The units of GJ and I_p are $\text{N} \cdot \text{m}^2$ and $\text{kg} \cdot \text{m}$, respectively. At the left-hand end, the bar is fixed to a torsional spring k_ϕ , representing the root boundary conditions. The units of k_ϕ are $\text{N} \cdot \text{m}/\text{rad}$. The torsional spring effect is generated by the presence of the induced strain actuator. At the right-hand side, the bar is connected to a tip inertia, I_o . The units of I_o are $\text{kg} \cdot \text{m}^2$.

Equation of Motion

The general equation of motion is given (Timoshenko, 1955; Inman, 1996) as:

$$-GJ\phi'' + I_p\ddot{\phi} = 0 \quad (2)$$

where $\phi = \phi(z, t)$ is the torsional rotation of the bar, and $\phi'' = \partial^2\phi/\partial x^2$, while $\ddot{\phi} = \partial^2\phi/\partial t^2$. Making the separation-of-variables assumption, yields

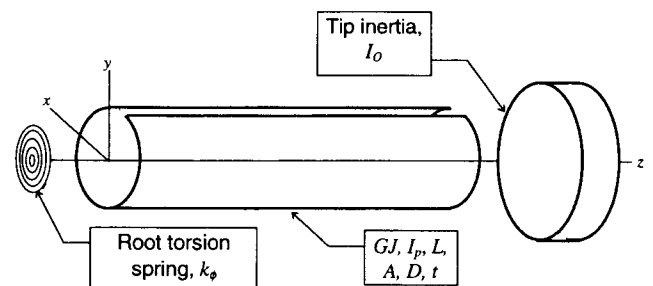


Figure 2. Schematic representation of the LARIS actuator as a torsional bar with finite stiffness at the root and concentrated rotary inertia at the tip.

$$\phi(z,t) = \Phi(z) \cdot e^{i\omega t} \tag{3}$$

and hence Equation (2) becomes:

$$GJ\Phi'' + \omega^2 I_p \Phi = 0 \tag{4}$$

Introducing the torsional wave speed,

$$c = \sqrt{\frac{GJ}{I_p}} \tag{5}$$

and the wavelength

$$\lambda = 2\pi \frac{c}{\omega} \tag{6}$$

yields

$$\Phi'' + \left(\frac{2\pi}{\lambda}\right)^2 I_p \Phi = 0 \tag{7}$$

General Solution

The general solution of Equation (7) is of the form

$$\Phi(z) = A \sin\left(2\pi \frac{z}{\lambda}\right) + B \cos\left(2\pi \frac{z}{\lambda}\right) \tag{8}$$

The constants A and B are determined from the boundary conditions.

Boundary Conditions

ROOT BOUNDARY CONDITION

The root boundary condition, represented by an elastic torsional restraint of stiffness k_ϕ , is expressed as

$$k_\phi \cdot \phi(0,t) = T(0,t) \tag{9}$$

where $T(0,t)$ is the torsional moment at $z = 0$. Using the elasticity relation

$$T(z,t) = GJ \cdot \phi'(z,t) \tag{10}$$

yields, for $z = 0$,

$$k_\phi \cdot \phi(0,t) = GJ \cdot \phi'(0,t) \tag{11}$$

Using the separation-of-variables assumption, we get

$$k_\phi \cdot \Phi(0) = GJ \cdot \Phi'(0) \tag{12}$$

TIP BOUNDARY CONDITION

The tip boundary, represented by the rotary inertia I_o , is expressed as

$$-T(L,t) = I_o \cdot \ddot{\phi}(L,t) \tag{13}$$

where the negative sign in front of $T(L,t)$ results from the sign convention. The elasticity Equation (10) yields

$$-GJ\phi'(L,t) = I_o \cdot \ddot{\phi}(L,t) \tag{14}$$

Using the separation-of-variables assumption, yields

$$GJ\Phi'(L) = \omega^2 I_o \cdot \Phi(L) \tag{15}$$

Characteristic Equation

Substituting the general solution into the boundary conditions yields an algebraic system of two equations in two unknowns that has as solution the constants A and B . The details of this process are as follows. First note that

$$\Phi(0) = B \tag{16}$$

$$\Phi'(0) = \frac{2\pi}{\lambda} A \tag{17}$$

$$\Phi(L) = A \sin\left(2\pi \frac{L}{\lambda}\right) + B \cos\left(2\pi \frac{L}{\lambda}\right) \tag{18}$$

$$\Phi'(L) = A \frac{2\pi}{\lambda} \cos\left(2\pi \frac{L}{\lambda}\right) - B \frac{2\pi}{\lambda} \sin\left(2\pi \frac{L}{\lambda}\right) \tag{19}$$

The root boundary condition yields

$$k_\phi B = GJ \frac{2\pi}{\lambda} A \tag{20}$$

i.e.,

$$A = \frac{k_\phi L}{GJ} \cdot \frac{\lambda}{2\pi L} B \tag{21}$$

Introduce the root stiffness coefficient

$$c_{k_\phi} = \frac{k_\phi L}{GJ} \tag{22}$$

and write

$$A = c_{k_\phi} \cdot \frac{\lambda}{2\pi L} B \tag{23}$$

Next, use the tip boundary condition to write

$$\begin{aligned} GJ \frac{2\pi}{\lambda} \left[A \cos \left(2\pi \frac{L}{\lambda} \right) - B \sin \left(2\pi \frac{L}{\lambda} \right) \right] \\ = I_o \omega^2 \cdot \left[A \sin \left(2\pi \frac{L}{\lambda} \right) + B \cos \left(2\pi \frac{L}{\lambda} \right) \right] \end{aligned} \quad (24)$$

Note that

$$\frac{I_o \omega^2 L}{GJ} = (2\pi)^2 \frac{GJ}{I_p \lambda^2} \cdot \frac{I_o L}{GJ} = \frac{I_o}{I_p L} \cdot \left(2\pi \frac{L}{\lambda} \right)^2 \quad (25)$$

Introduce the tip inertia coefficient

$$c_{I_o} = \frac{I_o}{I_p L} \quad (26)$$

and rearrange Equation (24) using Equation (23) to obtain the characteristic equation

$$\begin{aligned} \left[c_{k_\phi} \cos \left(2\pi \frac{L}{\lambda} \right) - 2\pi \frac{L}{\lambda} \sin \left(2\pi \frac{L}{\lambda} \right) \right] \\ = c_{I_o} \cdot 2\pi \frac{L}{\lambda} \left[c_{k_\phi} \sin \left(2\pi \frac{L}{\lambda} \right) + 2\pi \frac{L}{\lambda} \cos \left(2\pi \frac{L}{\lambda} \right) \right] \end{aligned} \quad (27)$$

Solution of the characteristic equation yields the characteristic torsional wavelength values, λ . Hence, the angular frequency, ω , is obtained as

$$\omega = \frac{2\pi}{\lambda} \sqrt{\frac{GJ}{I_p}} \quad (28)$$

To obtain the mode-shapes, we use Equation (23), for each value λ to get the value of A in terms of an unspecified value of B , and then express Equation (18) in terms of only one unknown, B . The value of B is found through the mode-shape normalization process, e.g., $\Phi(L) = 1$. The specific values of the root stiffness coefficient, c_{k_ϕ} , and the tip inertia coefficient, c_{I_o} are calculated from the design characteristics of the LARIS actuator and introduced in the characteristic Equation (27). The solution of Equation (27) is then obtained numerically.

Numerical Example

A parametric study was performed to illustrate the variation of the characteristic torsional wavelength values with the root stiffness coefficient, c_{k_ϕ} , and the tip inertia coefficient,

c_{I_o} . The characteristic Equation (27) was used to generate the characteristic function

$$\begin{aligned} f(\lambda) = \left[c_{k_\phi} \cos \left(2\pi \frac{L}{\lambda} \right) - 2\pi \frac{L}{\lambda} \sin \left(2\pi \frac{L}{\lambda} \right) \right] \\ - c_{I_o} \cdot 2\pi \frac{L}{\lambda} \left[c_{k_\phi} \sin \left(2\pi \frac{L}{\lambda} \right) + 2\pi \frac{L}{\lambda} \cos \left(2\pi \frac{L}{\lambda} \right) \right] \end{aligned} \quad (29)$$

The zeros of the characteristic function generate the values of the characteristic wavelength.

First, the characteristic function was verified by checking it in extreme situations for which closed form solution exists and can be readily derived or retrieved from the literature. Figure 3 shows graphs of the characteristic function for two such extreme cases: free-free and fixed-free. For both these cases, closed form solutions are available (Timoshenko, 1955; Inman, 1996), i.e.,

$$\lambda = \frac{2L}{n} \quad (\text{free-free}) \quad (30)$$

and

$$\lambda = \frac{4L}{(2n-1)} \quad (\text{fixed-free}) \quad (31)$$

These results can also be derived directly from Equation (27) by letting $c_{k_\phi} = 0$ and $c_{I_o} = 0$ (i.e., $K_\phi = 0$ and $I_o = 0$) for the free-free case, and $c_{k_\phi} \rightarrow \infty$ and $c_{I_o} = 0$ (i.e., $K_\phi \rightarrow \infty$ and $I_o = 0$) for the fixed-free case. Examination of Figure 3 gives a graphical confirmation of the fact that both these cases are zeros of the characteristic function given by Equation (29). Next, the tendency of variation of the characteristic wavelength with the values of tip inertia and root stiffness were examined for the free-free case. Figure 4 shows that the modification of tip inertia and root stiffness act in different ways.

A non-zero root stiffness creates a new characteristic L/λ value near zero. This can be explained if we consider that the free-free vibration has a hidden L/λ value at zero, i.e., for the motion corresponding to rigid body rotations. By addition of root stiffness, this zero L/λ value increases to a finite non-zero value. This leads to the apparent paradox that the addition of stiffness decreases the first characteristic root, and hence the first natural frequency! However, this apparent paradox has a completely valid explanation, since, in fact, the first root, that was zero, now gets a finite non-zero value. At higher root orders, the effect of root stiffness becomes much less pronounced.

The addition of tip inertia acts in the intuitive way, i.e., it decreases the first free-free vibration root, $L/\lambda = 0.5$. A clearer picture of the effects of root stiffness and tip inertia at

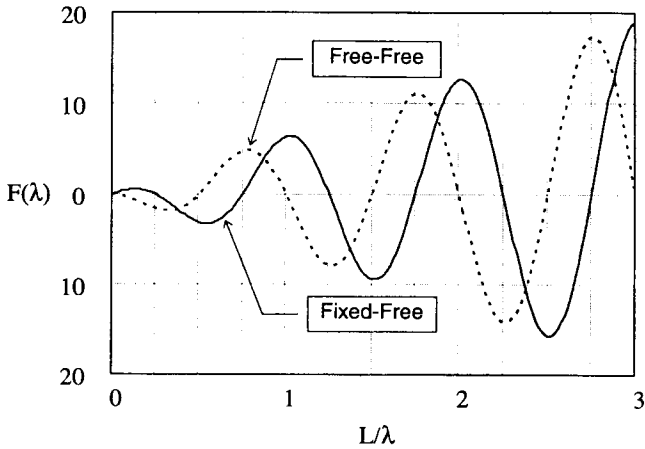


Figure 3. Graphs of the characteristic function for free-free and fixed-free boundary conditions.

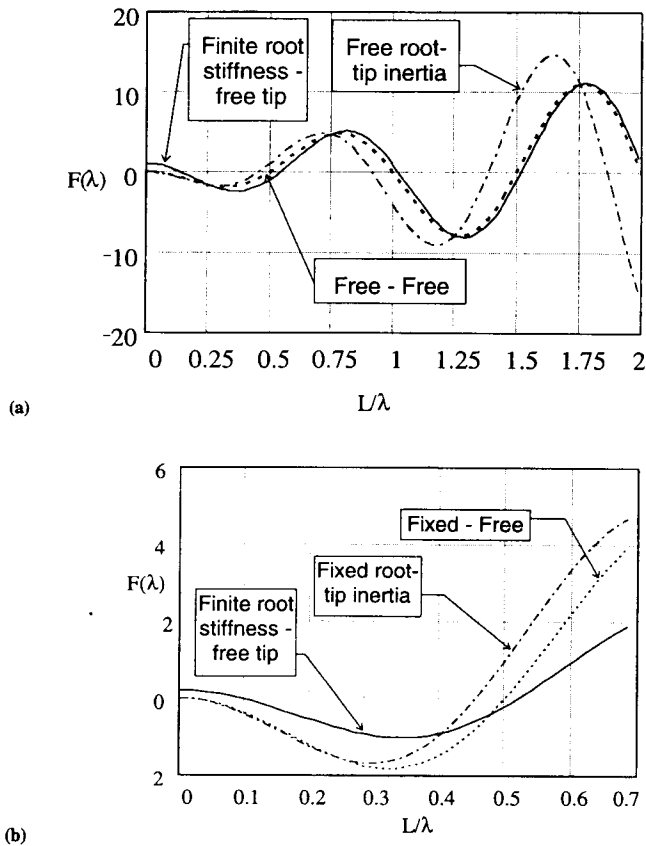


Figure 4. Graphs of the characteristic function for various combinations of tip inertia ($c_{I_0} = 0.1$) and root stiffness ($c_{K_0} = 0.4$) conditions: (a) range covering the first 4 characteristic roots; (b) details graph for the identification of the first characteristic root showing that addition of root stiffness creates an additional root near zero.

low root orders is given in the enlarged scale plot of Figure 4(b).

LARIS MK 2 DESIGN AND CONSTRUCTION

The design for the LARIS Mk 2 actuator was developed from the design of the LARIS Mk 1 proof-of-concept demonstrator. The LARIS Mk 1 actuator had four undesirable features:

1. It had a very poor dynamic performance manifesting violent lateral motion at frequencies below 10 Hz.
2. It did not have an angular indicator necessary for visual assessment of the output angular displacement.
3. The P-245.70 housing on the LARIS Mk 1 actuator exhibited parasitic lateral displacement whenever the translator was activated.
4. It lacked the compactness necessary for demonstrations traveling.

For LARIS Mk 2, the following design requirements were imposed:

- good dynamic performance with stable operation beyond 30 Hz
- portability to demonstration sites
- compact self-sustained construction

To achieve this, a number of new design items were considered:

- a stiff housing for the P-245.70 translator

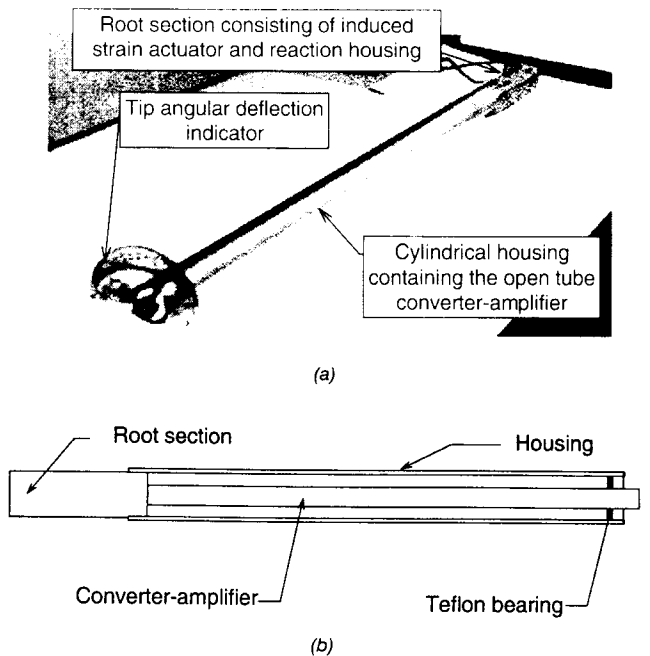


Figure 5. Description of LARIS Mk 2 actuator: (a) general lay-out; (b) cut-out schematic view showing the Teflon™ bearing support of the converter amplifier.

- an outer tube housing for the converter-amplifier that provides a bearing support at the free end
- an angular displacement indicator and protractor for the output displacement

The general lay-out of the LARIS Mk 2 actuator is given in Figure 5. It consists mainly of three parts: root section containing the induced-strain translator, cylindrical section containing the open-tube converter-amplifier, and tip section containing the angular deflection indicator. Details about the design and construction of LARIS Mk 2 actuator are given next.

Characteristics of the P-245.70 Induced-Strain Translator

The P-245.70 translator is commercially available from Polytec PI, Inc. This translator uses a stack of piezo-electric PZT ceramic proprietary produced by Polytec PI, Inc. Figure 6 shows dimensions and external appearance of this actuator. The characteristics of this translator, as resulting from the manufacturer’s catalogue, are reproduced in Table 1.

Selection of the Open Tube for LARIS Mk 2 Actuator

To keep within acceptable dimensional limits, the thin-wall open tube converter-amplifier was chosen around 1 m

long (1006 mm, exactly) with a nominal diameter of 25.4 mm. It was decided that the 1 m length would allow for easy placement of the LARIS Mk 2 actuator in an airplane overhead compartment or under its passenger seats.

Next, the tube material and wall thickness had to be selected. Commercially available thin-wall tubes, made of aluminum and stainless steel, were considered. The influence of the tube thickness and material properties on its stiffness, and hence on the angular displacement output, was calculated. This aspect is of great importance, since the effectiveness of induced strain actuators depends on the matching between the internal and external stiffness (k_i and k_e , respectively).

$$u_e = \frac{1}{1 + \frac{k_e}{k_i}} u_{ISA} \tag{32}$$

where

u_e = actuator effective output displacement under an applied load (mm)

u_{ISA} = actuator free displacement, i.e., under no external load (mm)

k_i = actuator internal stiffness (kN/mm)

k_e = external stiffness (N/mm)

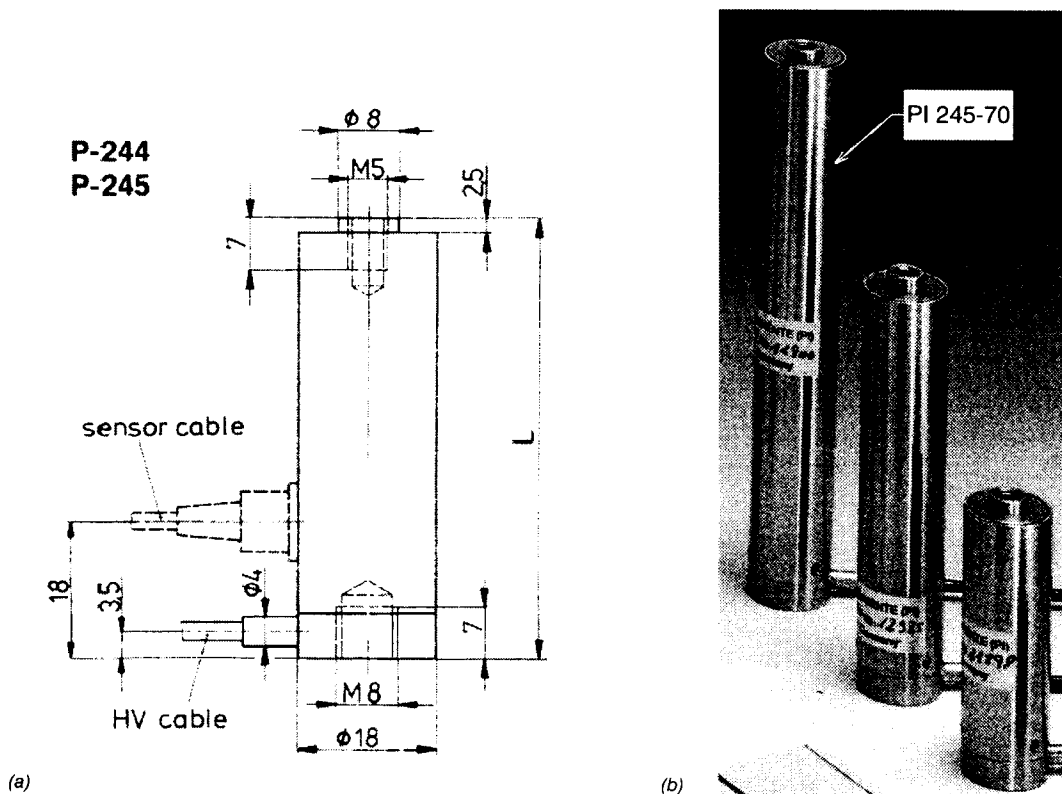


Figure 6. (a) Assembly drawing of P-245.70 translator. (b) Photograph of the P-245.XX translator family (courtesy Polytec PI, Inc.).

Table 1. Technical characteristics of the P-245.70 translator.

| | |
|------------------------------|---------------------|
| Price | \$1450 |
| Nominal voltage | -1000 V |
| Polarity | negative |
| Max. pushing force | 1000 N |
| Max. pulling force | 300 N |
| Temperature range | TS (-40°C to +80°C) |
| Max. expansion (at -1000 V) | 120 μ m |
| Stiffness | 8 N/ μ m |
| Electrical capacitance | 450 nF |
| Resonant frequency | 5 kHz |
| Total length (± 0.5 mm) | 124 mm |

To the induced-strain piezoelectric translator PI 245.70, the open-tube converter-amplifier acts as an external stiffness of value k_c . At the point of contact, the torsional stiffness of the open tube is seen by the induced-strain translator as an equivalent linear stiffness given by:

$$k_c = \left(\frac{L}{2A} \right)^2 \frac{GJ}{L} \quad (33)$$

where

L = tube length (mm)

A = tube's enclosed area, $\pi D^2/4$ (mm²)

GJ = torsional stiffness, $G\pi D^3/3$ (MPa \cdot mm²)

Table 2 shows a summary of the analysis performed on four tubes of the same length and diameter, but of different materials and wall thickness. The analysis was performed for the maximum nominal free displacement of the P-245.70 translator, $u_{NSA} = 0.120$ mm, and for its internal stiffness, $k_i = 8000$ N/mm. The predicted angular displacement was calculated using Equations (1), (32) and (33).

As shown by the data in Table 2, an increase in the wall thickness of the aluminum and stainless steel tubes results in an increase in their stiffness and a decrease of the output angular displacement of the LARIS device. Eventually, we selected two aluminum tubes (#3 and #4) for use in the construction of the LARIS Mk 2 actuator, because of their low weight and high effectiveness.

The two different thickness values were selected to illustrate the effect that an increase in tube thickness will have on

the resulting stiffness, angular displacement output, and natural frequency. It is important to note that, as described in a future section, the static test of the LARIS actuator using the 0.89 mm thick aluminum tube as the converter/amplifier revealed a maximum nominal angular displacement value of 6 degrees. This value is within 5.5 percent of the theoretical value of 6.35 degrees. The selected tubes were bought on the commercial market and the longitudinal slits were milled at MTD, Inc. in Blacksburg, Virginia.

Box Housing for the P-245.70 Translator

Under operation of the initial LARIS Mk 1 actuator, it was found that aluminum housing for the P-245.70 translator exhibited parasitic lateral displacement. Figure 7 indicates the back and forth direction of this unwanted motion. To stop this motion, a five-sided, 0.953 cm thick (3/8 inch), 20.3 cm long (8 inches), and 3.62 cm wide (1.425 inches) aluminum box was designed and built (Figure 8). This box was assembled with fifteen 0.2160"-24 UNC screws. It was predicted that the closed box design of this new housing would provide the necessary stiffness for the elimination of the unwanted parasitic lateral motion. Subsequent static and dynamic tests of the LARIS actuator revealed that this was indeed so.

Cylindrical Housing for the Converter-Amplifier

The 1-inch diameter converter/amplifier tube was placed into an outer 2-inch (50.8 mm) tube that served as housing and tip support. This outer tube is fastened to the P-245.70 box housing with the three 0.375" long, 0.1900"-24 UNC screws. This cylindrical housing serves two purposes. One is to provide stationary support for a 1-inch Teflon™ ring that acts as a bearing support for the inner 1-inch diameter converter/amplifier tube. The other is to serve as reference base for measuring the angular displacement output.

Angular Displacement Indicator

An angular displacement indicator was fixed to the cylindrical housing of the LARIS Mk 2 actuator (Figure 9). The angular displacement indicator consisted of a light arrow fixed to the inner converter/amplifier tube, and a protractor fixed to the outer housing.

Table 2. Summary of the design analysis performed to select the converter-amplifier open tube for the LARIS Mk 2 actuator.

| # | Material Type | Shear Modulus, G (MPa) | Tube Thickness, t (mm) | Tube Stiffness, k_c (N/mm) | Relative Displacement, Δw (mm) | Angular Displacement, δ (degrees) |
|---|-----------------|------------------------|------------------------|------------------------------|--|--|
| 1 | Stainless steel | 80,000 | 1.24 | 3950 | 0.080 | 4.54 |
| 2 | Stainless steel | 80,000 | 1.65 | 9307 | 0.055 | 3.14 |
| 3 | Aluminum | 30,000 | 0.89 | 548 | 0.112 | 6.35 |
| 4 | Aluminum | 30,000 | 1.65 | 3490 | 0.084 | 4.72 |

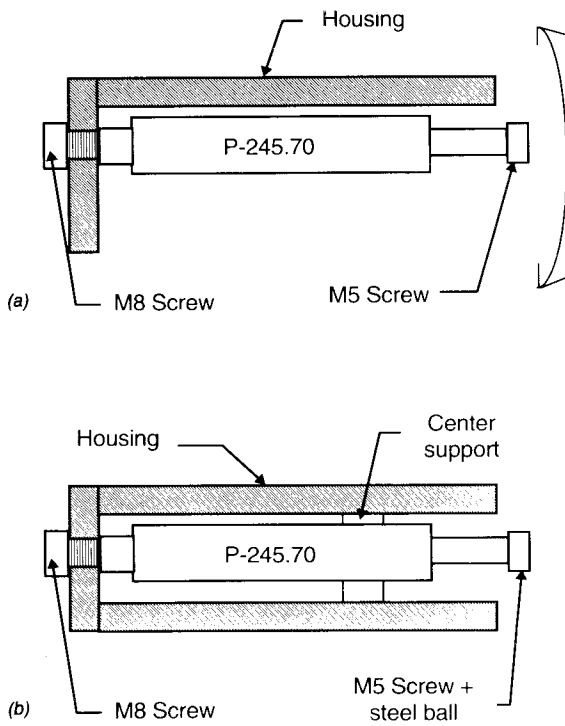


Figure 7. Unwanted lateral displacement of the LARIS Mk 1 actuator.

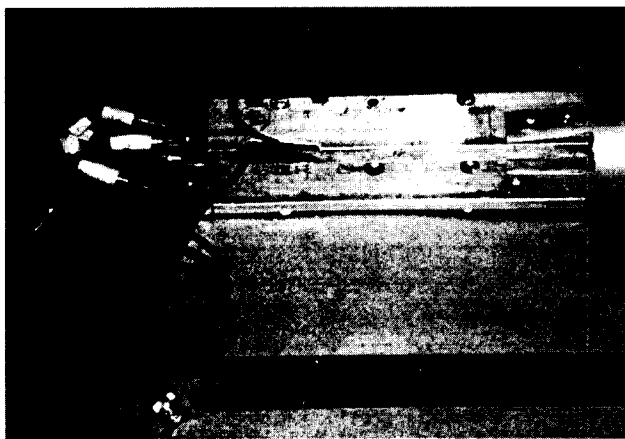


Figure 8. Box housing for the P-245.70 translator placed at the root of the LARIS Mk 2 actuator.

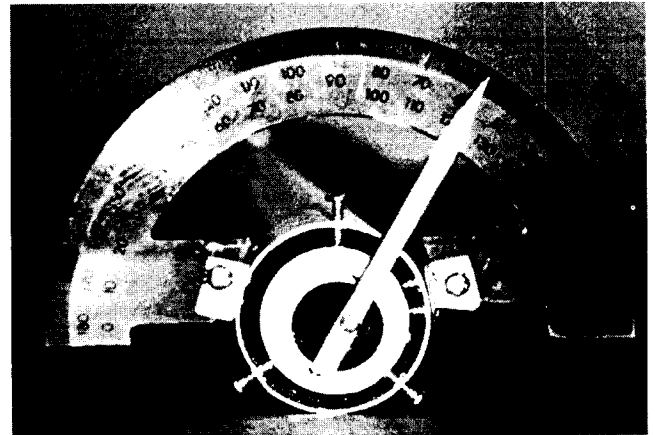


Figure 9. Detail of the angular displacement indicator placed at the tip of the LARIS Mk 2 actuator.

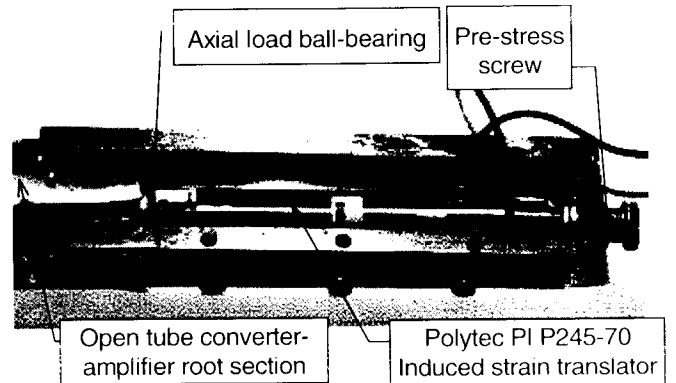


Figure 10. Detail of the box housing for the P-245.70 induced strain translator placed at the root of the LARIS Mk 2 actuator.

Central Application of the Axial Force

A two-inch long triangular piece was used to transmit the axial force into the root section of the converter-amplifier. Through this piece, the tip of the P-245.70 applied the actuation force to the moving side of the open-tube converter-amplifier (Figure 10). The force was applied at a position corresponding to the center of the converter-amplifier tube. An M5 screw with a central recess and a small steel ball bearing were used to create a proper frictionless interface for the transmission of this force. This ball bearing interface also provides a placement guide for coupling of the P-245.70 translator to the open-tube converter-amplifier.

EXPERIMENTAL SET-UP FOR STATIC AND DYNAMIC TESTING OF LARIS Mk 2 ACTUATOR

The experimental set-up for static and dynamic testing is shown in Figure 11. The instrumentation consisted of two main groups: excitation equipment and measuring equipment.

The excitation equipment included:

- Hewlett-Packard HP 3314A function generator
- Trek 50/750 dual-channel high voltage amplifier

The measuring equipment consisted of:

- JDR Model 2000 oscilloscope for measuring the low-voltage and high-voltage excitation signals

- X10 oscilloscope probe to reduce the high-voltage excitation signal by a factor of 10 in order to come within the oscilloscope range
- Schlumberger Industries DF 1.0 linear displacement transducer
- Hewlett Packard 62128A DC power supply for the excitation of the DF 1.0 transducer
- Micronta digital multimeter for measuring the displacement transducer output in static regime
- Tektronix 2205 Oscilloscope for displaying the signal from the DF 1.0 displacement transducer in dynamic regime

The displacement transducer was mounted at the tip of the LARIS actuator and fixed to its casing at a radial position $d = 14$ mm from the center. Through this set-up, the angular motion of the indicator arm was measured as a linear displacement of the DF 1.0 transducer armature. The moving armature of the displacement transducer was fixed perpendicular to the indicator arm with an elastomeric material that could adjust for the slight angular movements connected with the angle measurements.

STATIC TESTING OF LARIS Mk 2 ACTUATOR

The static testing of the LARIS Mk 2 actuator was performed in order to verify the results of the static analysis and to determine the maximum angular capability of the actuator. These tests were in many respects similar to the initial tests

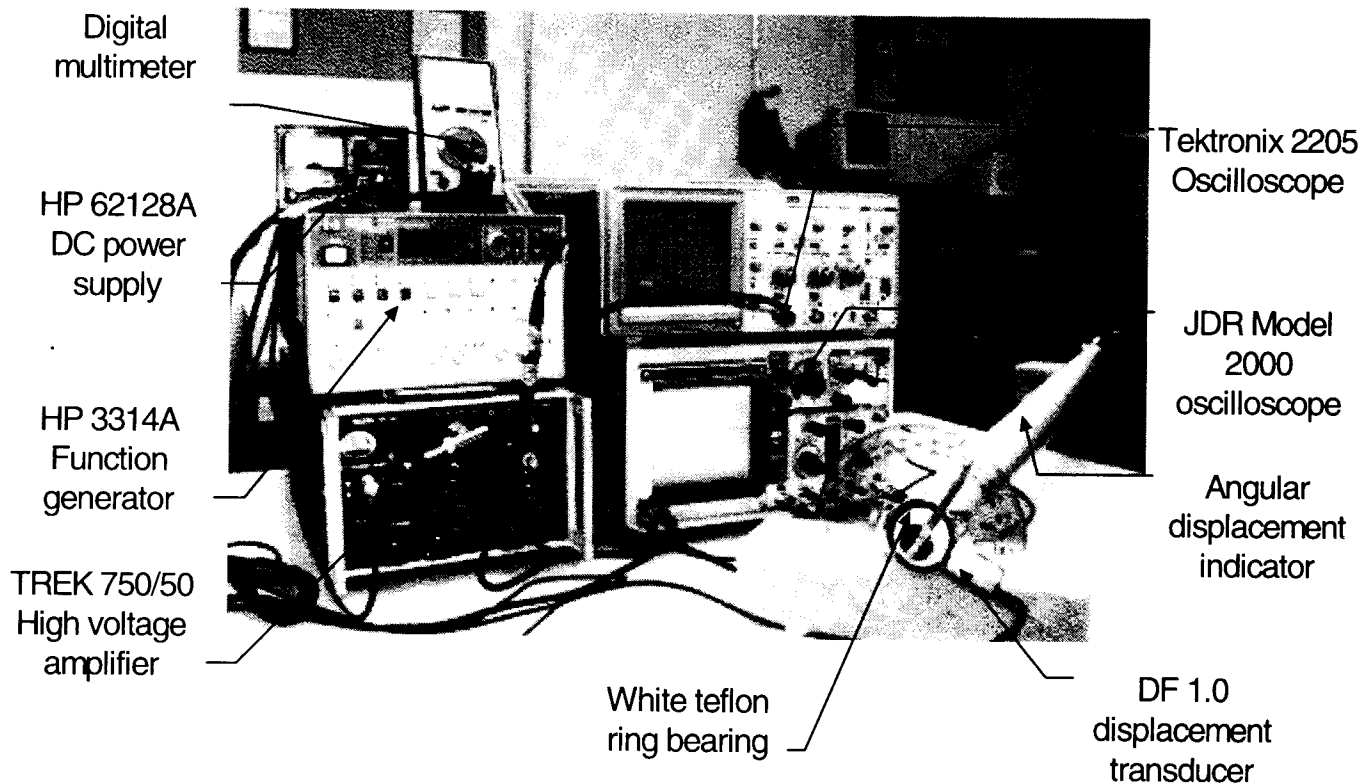


Figure 11. General lay-out for the static and dynamic testing of the LARIS Mk 2 actuator.

performed on the LARIS Mk 1 actuator and reported by Giurgiutiu et al. (1996, 1997). Due to the similarity of the results to those already published, these static experiments will not be detailed here. The main results of the static experiments, that confirmed the theoretical predictions, was that the LARIS output angular displacement can be expressed in the form

$$\phi = (1 - e^{-L/L_0}) \left(\phi'_0 + \frac{L}{2A} \right) \Delta w \quad (34)$$

where ϕ'_0 is a zero off-set term, and L_0 is a length scale. This theoretical model represents an improvement over the simple linear theory. At large distances from the built-in root, the model displays the linear proportionality between angular output displacement, ϕ , and linear induced-strain input, Δw . However, close to the root, the model allows for an exponential decay function that accounts for the restrained warping effects.

For the open tube geometry employed in these tests, a maximum angular deflection of 6° was measured. This angular deflection is equivalent to the 8° deflection reported for the LARIS Mk 1 model since the length of the Mk 2 model was smaller than that of the Mk 1. As expected, the output displacement is proportional to the actuator length.

DYNAMIC TESTING OF LARIS MK 2 ACTUATOR

The LARIS Mk 2 actuator was subjected to intensive dynamic testing in order to determine its frequency response over the 0–50 Hz frequency range of interest. Figure 11 shows the test setup. The test was conducted by applying a +100 to –1000 V sinusoidal signal to the P-245.70 induced strain actuator. Forcing frequencies were varied from 0.5 Hz to 1 Hz and then in 1 Hz steps up to 50 Hz. At each forcing frequency, linear displacement measurements were taken using the DF 1.0 transducer and the Tektronix 2205 oscilloscope. These measurements were later converted to angular displacement values using:

$$\phi = \sin^{-1} \left(\frac{\Delta l}{d} \right) \quad (35)$$

where $d = 14$ mm is the rotor arm. During the tests, it was observed that the output displacement remained at constant amplitude over a large frequency range. In fact, a change in output displacement amplitude started to become noticeable only above 40 Hz, when an increasing response, indicative of incoming resonance, was observed. For this reason, the test was stopped at 50 Hz in order to avoid destruction of the experimental apparatus through undamped resonance response.

Figure 12 presents the dynamic test results as a plot of output displacement amplitude versus frequency. This plot shows the same general tendencies that resulted from direct

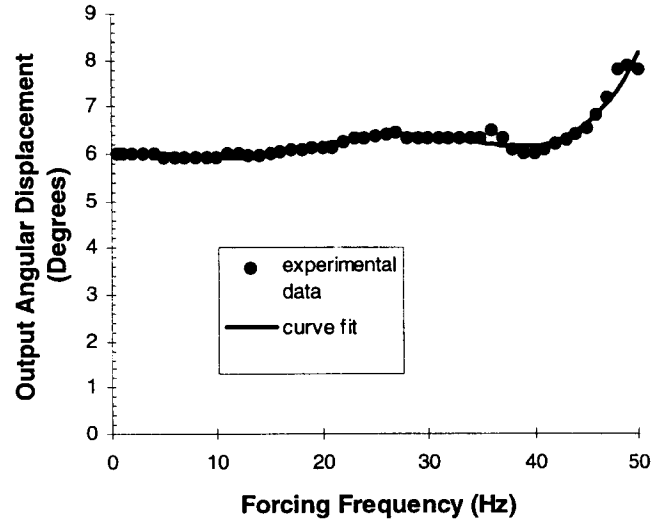


Figure 12. Angular displacement response of the LARIS Mk 2 actuator at various frequencies in the range 0.5–50 Hz.

observation during the test. Up to approximately 40 Hz, nothing significant happens, and the output amplitude stays constant close to the static values of 6° . If a variation is to be found at all, that variation seems to be a slight increase in amplitude over the static value. This increase can be attributed to friction reduction due to sustained motion. Starting at approximately 40 Hz, a marked increase of amplitude with frequency is observed. Beyond 45 Hz, this increase becomes very sharp and pronounced, indicative of the proximity of a resonance. The tests were interrupted at 50 Hz, which is before the actual resonance. However, from the general shape of the frequency response curve it can be inferred that the actual resonance frequency is in the range 50–60 Hz. In lieu of measured data, a good estimate of the resonance frequency would be $f_{exp} = 55$ Hz.

COMPARISON OF EXPERIMENTAL RESULTS AND THEORETICAL PREDICTIONS

An estimate of the resonance frequency can be obtained using the roots of the characteristic equation developed in the theoretical section, and the geometric dimensions and elastic properties of the LARIS Mk 2 actuator. Modeling of the LARIS Mk 2 actuator yielded the following parameters:

$$L = 1000 \text{ mm}, \quad D = 25.4 \text{ mm}, \quad t = 0.889 \text{ mm}$$

$$A = 506.7 \text{ mm}, \quad J = 18.7 \text{ mm}^4, \quad G = 27 \text{ GPa}$$

$$\rho = 2.7 \times 10^6, \quad I_p = 0.0309 \text{ Kg mm}$$

Substitution in the torsional wavespeed equation yields:

$$c = \sqrt{\frac{GJ}{I_p}} = 128 \text{ m/s} \quad (36)$$

For $c_{k\phi} = 0$ and $c_{I_0} = 0.1$, the numerical solution of the characteristic equation yields the wavelength ratio:

$$\frac{L}{\lambda} = 0.45 \quad (37)$$

Hence, the predicted frequency is

$$f_{th} = \frac{c}{\lambda} = 0.45 \frac{c}{L} = 57.6 \text{ Hz} \quad (38)$$

The predicted frequency, $f_{th} = 57.6$ Hz, and the experimental frequency, $f_{exp} = 55$ Hz, are sufficiently close, considering that the resonance condition could not be measured.

COMMENTS AND CONCLUSIONS

The results presented in this paper show that the LARIS Mk 2 actuator exhibits marked performance improvements in comparison to the previously tested LARIS Mk 1 proof-of-concept demonstrator (Giurgiutiu and Rogers, 1997). The static and dynamic tests performed on the LARIS Mk 2 actuator showed very good behavior in the frequency range 0–50 Hz. Below 40 Hz, the frequency response curve was flat, thus indicating a very good actuator response. Above 40 Hz, the frequency response curve showed a tendency of monotonic amplitude increase, indicative of approaching a mechanical resonance. However, this resonance lies outside the tested interval 0–50 Hz. As a result of these tests, the frequency interval 0–50 Hz was verified to be secure for safe operation of the LARIS Mk 2 actuator. The performance improvements detailed in this paper are a direct result of the analysis and design efforts invested in the construction and testing of this new series of LARIS actuators.

The paper also presents a general methodology for the analysis of torsional vibrations of uniform bars that have simultaneously distributed and concentrated stiffness and inertia properties. Unlike previous developments (Timoshenko, 1955; Inman, 1996), this analysis develops the general solution in terms of the torsional vibrations wave-speed and the characteristic wavelength. In our research, this general methodology was used to perform the dynamic analysis of the LARIS Mk 2 actuator, which, besides its distributed parameters, has concentrated torsional stiffness at the root, and concentrated torsional inertia at the tip. However, the analysis methodology is versatile and is not restricted to the LARIS concept. This methodology can also be used for the analysis and design of other torsional devices that present a mixture of distributed and concentrated mass and stiffness characteristics. The theoretical predictions and experimental results described in this paper show good nu-

merical correlation and confirm that the theoretical assumptions and conceptual developments are valid.

The theoretical and experimental work described in this paper concludes the initial exploratory phase of the LARIS actuator development. The next phase in this challenging research topic should concentrate on building a LARIS actuator tailored to meet specific operational requirements for a full-scale real-life application. A series of aerospace and mechanical engineering applications are considered, such as: adaptive control surfaces for aircraft wings and helicopter blades; active noise and vibration suppression of helicopter rotor blades; flutter and vibration suppression of fighter aircraft wings and tailplanes; gust alleviation devices for transport aircraft; rotary vane actuators in the control of turbomachinery exhaust flow for active reduction turbulence, noise, and vibrations.

ACKNOWLEDGEMENT

The authors gratefully acknowledge the support of Army Research Office—University Research Initiative Program, Grant No. DAAL 03-92-0181, Dr. Gary Anderson, Program Manager.

REFERENCES

- Bernhard, A. P. F. and I. Chopra. 1996. "Hover Testing of a Smart Flap Activated by a Bending-Torsion Coupled Beam", *Proceedings of the 37th AIAA/ASME/ASCE/AHS/ASC Structures, Structural Dynamics and Materials Conference and Adaptive Structures Forum*, Salt Lake City, UT, April 15–19, #AIAA-946-11272-CP.
- Bothwell, C. M., R. Chadra and I. Chopra. 1994. "Torsional Actuation with Extension-Torsion Composite Coupling and Magnetostrictive Actuators", *Proceedings of the 35th AIAA/ASME/ASCE/AHS/ASC Structures, Structural Dynamics and Materials Conference and Adaptive Structures Forum*, Hilton Head, SC, April 18–21, #AIAA-94-1760-CP.
- Chen, P. C. and I. Chopra. 1993. "A Feasibility Study to Build a Smart Rotor: Induced-Strain Actuation of Airfoil Twisting Using Piezoceramics", *Proceedings of the 1993 North American Conference on Smart Structures and Materials*, Paper 1917-1920, Hyatt Regency Hotel, Albuquerque, NM, January 31–February 4.
- Giurgiutiu, V. and C. A. Rogers. 1997. "Large-Amplitude Rotary Induced-Strain (LARIS) Actuator", *Journal of Intelligent Material Systems and Structures*, Technomic Publishing Co. (in press).
- Giurgiutiu, V., Z. Chaudhry and C. A. Rogers. 1996. "Energy-Based Comparison of Solid-State Induced-Strain Actuators", *Journal of Intelligent Material Systems and Structures*, Technomic Publishing Co., 7(1):4–14.
- Giurgiutiu, V., Z. Chaudhry and C. A. Rogers. 1994. "Engineering Feasibility of Induced-Strain Actuators for Rotor Blade Active Vibration Control", *Smart Structures and Materials 1994*, Orlando, FL, February 13–18, *SPIE*, 2190-11, 2190:107–122.
- Inman, D. J. 1996. *Engineering Vibration*, Prentice Hall.
- Straub, K. and R. King. 1996. "Applications of Smart Materials to Control of a Helicopter Rotor", *Smart Structures and Materials 1996—Industrial and Commercial Applications of Smart Structures Technology*, *SPIE*, 2721:66–77.
- Timoshenko, S. 1955. *Vibration Problems in Engineering*, 3rd Edition, Van Nostrand.